LBNL-42791

ERNEST ORLANDO LAWRENCE
BERKELEY NATIONAL LABORATORY

Acoustic Detection of Immiscible Liquids in Unconsolidated Sand

Jil T. Geller, Michael B. Kowalsky,
Patricia K. Seifert, and Kurt T. Nihei

Earth Sciences Division

March 1999

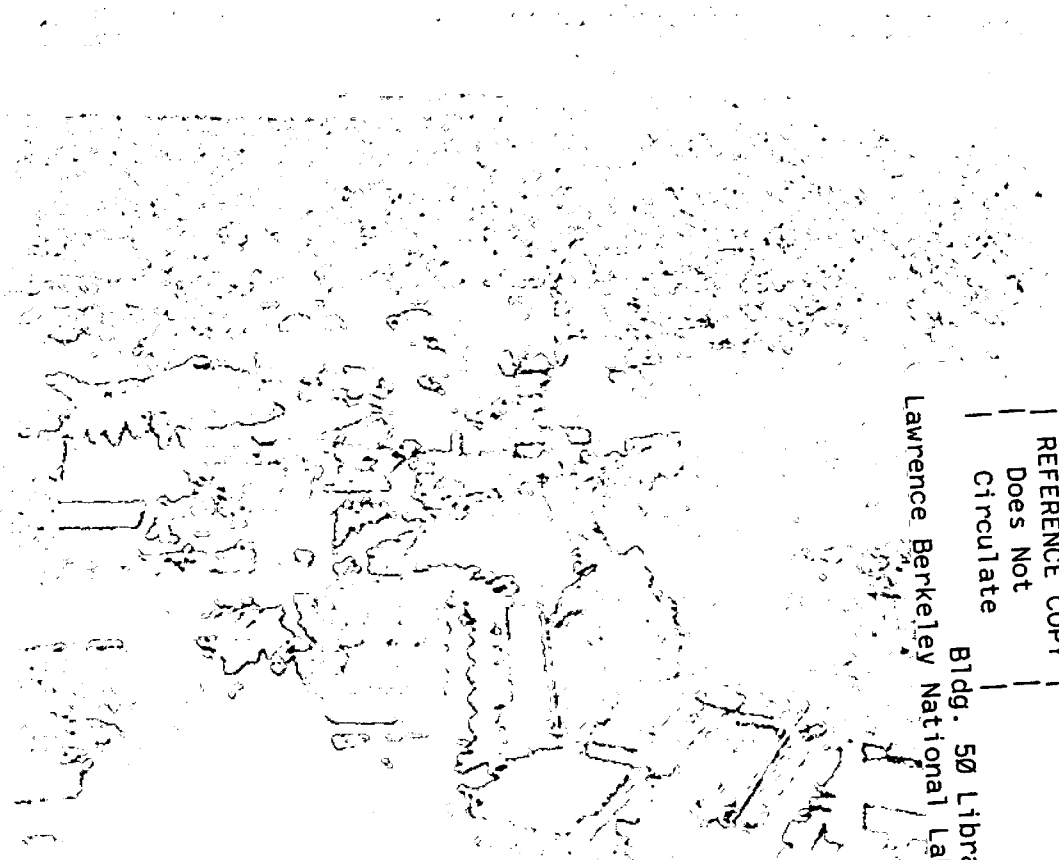

DISCLAIMER

LBNL-42791

Acoustic detection of immiscible liquids in unconsolidated sand

Jil T. Geller[1], Michael B. Kowalsky[2], Patricia K. Seifert[3] and Kurt T. Nihei[1]

[1]Earth Sciences Division, Ernest Orlando Lawrence Berkeley National Laboratory, Berkeley, California

[2]Department of Civil and Environmental Engineering, University of California, Berkeley, California

[3]Department of Geology and Geophysics, University of California, Berkeley, California (now at McKinsey Corporation, Munich, Germany)

March 1999

This work was sponsored by the Director, Office of Energy Research, Office of Basic Energy Sciences, Geosciences Program, through U.S. Department of Energy contracts DE-AC03-76F00098 and DEF602-93ER14391 and by the Air Force Office of Scientific Research, USAF, under grant/contract number FQ8671-96-0-1169

Abstract

Laboratory cross-well P-wave transmission at 90 kHz was measured in a 61 cm diameter by 76 cm tall water-saturated sand pack, before and after introducing a non-aqueous phase organic liquid (NAPL) (n-dodecane). In one experiment, NAPL was introduced to form a lens trapped by a low permeability layer; a second experiment considered NAPL residual trapped behind the front of flowing NAPL. The NAPL caused significant changes in the travel time and amplitude of first arrivals, as well as the generation of diffracted waves arriving after the direct wave. The spatial variations in NAPL saturation obtained from excavation at the end of the experiment correlated well with the observed variations in the P-wave amplitudes and travel times. NAPL residual saturation changes from NAPL flow channels of 3 to 4 % were detectable and the 40 to 80% NAPL saturation in the NAPL lens was clearly visible at acoustic frequencies. The results of these experiments demonstrate that small NAPL saturations may be more easily detected with amplitude rather than travel time data, but that the relationships between the amplitude changes and NAPL saturation may be more complex than those for velocity.

Introduction

Detecting and characterizing the distribution of immiscible liquids in unconsolidated sands is important for energy resource recovery and remediation of contaminated groundwater aquifers. Both petroleum products and organic liquid solvents are ubiquitous ground water contaminants that persist as non-aqueous phase liquids (NAPLs), owing to their low solubilities in water, and are source terms for extensive volatile organic chemical plumes. Seismic tomography may be an economically beneficial, non-invasive technique for mapping and monitoring the distribution of immiscible liquids between boreholes.

Significant changes in P-wave velocity and attenuation were measured in unconsolidated sand columns at 500 kHz due to the presence of varying fractions of water and NAPLs (Geller and Myer, 1995). Geller and Myer measured an approximately linear relationship between P-wave velocity and NAPL saturation and modeled it with simple mixing laws of the bulk-moduli of the liquid and solid phases (Kuster and Toksöz, 1974) for NAPLs of different densities and viscosities. However, the relationship between P-wave amplitudes and NAPL saturation was much more complex. The effect of the NAPL on energy attenuation was consistently greater than the effect on velocity. Furthermore, while P-wave velocity was sensitive to the volume fraction of NAPL, attenuation was also sensitive to its distribution. These results have motivated our continued investigation of attenuation as a potentially more revealing attribute for mapping NAPL distributions.

For the case of homogeneously-distributed NAPL residual, Seifert et al. (1998) predicted measured velocity and attenuation changes by modeling one-dimensional scattering from stacks of water-NAPL-sand interfaces. However, this model under-predicted the magnitude of attenuation for heterogeneous, or "patchy", NAPL distributions arising from unstable displacement conditions where NAPL flowed through the column in narrow channels (as opposed to a uniform front). The case of heterogeneous and patchy NAPL distributions is more relevant to field conditions, as a result of both flow instabilities and media heterogeneities.

While the velocity trends are expected to be consistent at lower frequencies, energy attenuation may be strongly frequency-dependent. In this paper we describe a series of experiments conducted to measure the detectability of NAPLs by P-waves at a frequency range that is one order of magnitude lower than in the column studies.

Description of Experiments

Two NAPL injection experiments were performed in a 61-cm diameter by 76-cm tall tank (Fig. 1), constructed of steel pipe with welded flanges and 25.4-mm aluminum top and bottom plates. The tank is lined with a 3-mm thick neoprene rubber jacket to allow the application of confining pressures up to 0.5 MPa. Six 3-cm diameter acrylic wells are located just inside the vessel wall for the cross-well acoustic data acquisition. The top and bottom plates have ports for fluid injection and drainage.

In each experiment, the tank was packed with well-sorted dry sand by pluviation from a constant height of fall and at a constant flow rate. The packed tank was saturated with de-aired tap water injected from the tank bottom after flushing with CO_2. n-Dodecane (DX2420-3, EM Science, Gibbstown, NJ), a lighter-than-water NAPL, was injected from the bottom of the tank with a peristaltic pump (Masterflex console drive, pump 7021-24, Cole Parmer, Chicago, IL). n-Dodecane has a specific gravity of 0.745 and a viscosity of 1.378 kPa-s (slightly more viscous than water; Riddick and Bunger, 1970). The acoustic velocity of n-dodecane is 1,290 m/s (22°C, Wang and Nur, 1991), which is 14% lower than that of water. By injecting from the bottom of the tank, buoyancy forces drive the NAPL to channel upward, leaving residual NAPL segments along the flow paths. This distribution is analogous to the distribution created by the downward migration of denser-than-water NAPL contaminants in groundwater aquifers. Oil Red O dye (Sigma Chemical Co., St. Louis, MO) was added at 0.5 g/L so that the NAPL distribution could be mapped after the experiment by excavation. The surface tension of the dyed n-dodecane and the interfacial tension of n-dodecane and tap water were 25.1 and 38.8 dynes/cm, respectively, measured with a ring tensiometer (CSC-Du Nouy, No. 7053, Fairfax, VA).

The cross-well seismic data is obtained using source and receiver tools mounted in acrylic tubes that are water-coupled to the borehole wall through a water annulus trapped between two O-rings, allowing the rest of the borehole to remain dry. This configuration prevents the generation of borehole tube waves. The source consists of a bar piezoelectric crystal (PZT 5400 Navy I; resonance frequency 123 kHz) that is excited by a 90 kHz single-cycle tone amplified to 50 V peak-to-peak. This frequency corresponds to P-wave wavelengths in the water-saturated sand of approximately 2 cm. The receivers are high frequency accelerometers (PCB 309A; resonance frequency >120 kHz) oriented horizontally in the plane of the cross-well experiment. The waveforms from the accelerometers are preamplified to 40 dB, stacked 60 to 100 times and stored on the hard drive of a digital oscilloscope (LeCroy, LC334AM, Chestnut Ridge, NY). Scanning across the tank diameter between one pair of boreholes was performed manually before and after the NAPL injection by moving the source and receiver tools in vertical increments of 1 cm. This interval is approximately equal to 1/2 the wavelength of the received P-wave.

At the end of the experiment, the three-dimensional distribution of the NAPL was measured by excavation. A thin-walled brass grid with 5 x 5 x 10 cm-deep cells covering the horizontal cross-sectional area of the tank was pressed down into the sand/water/dodecane mixture which was collected from each cell. Layers of approximately 5 cm in depth were excavated consecutively. The NAPL volume in the samples taken from the plane of the scan was measured by extracting the dyed NAPL into a known volume of clean n-dodecane and measuring the resulting dye concentration with a UV spectrophotometer (Hach DR/2000, Loveland, CO). The sand collected in each grid cell was oven dried and weighed in order to calculate the NAPL saturation using the bulk porosity. In Experiment A, several layers of the sand pack were excavated by freezing. Liquid nitrogen was poured over the cross-sectional area of the tank, and then the frozen portion was lifted from the tank. This method disturbed facilitated the removal of the larger quantities of NAPL near the top of the coarse sand, however it could only provide an average value of NAPL saturation at a given tank depth.

Experiment A tested the acoustic response to the presence of a NAPL lens (Fig. 1a). The bottom 52.6 cm of the tank was packed with a coarse, sub-rounded 12/20 mesh (0.85 mm – 1.7 mm grain diameter) quartz sand (Unamin Corp., LeSuer, MN) to a porosity of 0.34. A 25-cm thick layer of 44 to 88 μm diameter glass beads (MS-ML 105-53 glass-shot beads, Smith Industrial Supplies, San Lorenzo, CA) was placed over the sand to form a capillary barrier to the upward flowing NAPL and promote the formation of a NAPL lens within the coarse sand. No confining pressure was applied in this test. The NAPL was injected through a 7.3 cm diameter flow distribution disc at a height of 20 cm above the tank bottom. A total of 6.7 L of NAPL was injected at a flow rate of 94 mL/hr over 3 days. The fact that only water was collected from the top plate ports indicated that the capillary barrier kept all of the injected NAPL within the coarse sand.

Experiment B (Kowalsky et al., 1998) measured the response to the presence of NAPL residual (Fig. 1b). The entire tank was packed with angular 12 mesh quartz sand (#2/12, RMC Lonestar, Pleasanton, CA). A confining pressure of 0.14 MPa was applied after the sand was water-saturated, while allowing the pore-water to drain. The packed tank porosity under confining pressure was estimated to be 0.3, based upon the mass of sand, the tank volume and the volume of water drained. The NAPL was injected through four 1.6-mm I.D. stainless steel tubes equally spaced 7.5 cm from the tank's vertical axis and approximately 20 cm from the tank bottom. After 2.5 hours of NAPL injection at 30 mL/hr, the NAPL broke through one of the three open ports on the tank top. This early breakthrough indicated that the NAPL was flowing through one to several narrow channels. The flow rate was then increased to approximately 360 mL/hr to promote the development of additional NAPL flow paths. The injection was monitored from a fixed source and receiver location with time-lapsed, zero-offset, transmitted P-waves. The P-wave amplitudes decreased by approximately 35% during injection and recovered to 23% of the baseline value after the injection stopped, presumably due to redistribution of the NAPL. The mass balance of NAPL injected into the tank and collected in the effluent indicated 595 mL of NAPL was trapped in the sand. A second crosshole data set was collected following the NAPL injection.

Results

In this paper, we report the zero-offset scans from the two experiments and the measured NAPL distributions. In zero-offset measurements, the source and receiver are kept at equal depths as they are moved down the boreholes through the scanning region, therefore providing horizontally-averaged measurements. Tomographic inversion of the data sets to reveal both horizontal and vertical distributions of seismic attributes is ongoing and will be published separately. The results of two tomographic inversion methods have been reported to date using the data from Experiment B: straight-ray velocity tomography by Kowalsky et al. (1998) and asymptotic waveform inversion by Keers et al. (1999).

The zero-offset scans for Experiment A are shown in Figure 2. The first change in amplitude along the time axis is due to the first arrival of the P-wave (or travel time) and is indicated by arrow A in Figure 2a. This travel time is used to compute the P-wave velocity. Two other arrivals, indicated with arrows B and C, are the back and side-wall reflections, respectively. The reference scan (for the water-saturated tank) shows attenuation and diffraction due to the

glass bead/sand interface (Fig. 2a). This interface is not sharp, and includes a transitional region of about two to three cm where the smaller diameter beads fill the pore space of the coarse sand. The relatively smaller amplitudes in the glass-bead layer indicate that it may not have been completely saturated with water, due to its extremely small pore-size preventing the complete removal of entrapped air. The post-injection scan (Fig. 2b) shows a significant delay in the first arrival time and decrease in amplitude below the glass-bead/sand interface; the depth at which these attributes recover delineates the bottom of the NAPL lens. In addition, changes in arrival times and amplitudes occur within the NAPL layer. Much smaller changes in both amplitude and diffraction patterns after the first arrival can also be seen below the NAPL lens, due to the NAPL residual.

Figures 2(c) and (d) show the variation in travel times (corrected for the time delay for travel through the boreholes) and amplitudes, respectively, over the depth of the tank before and after NAPL injection. Within the coarse sand away from the sand/bead interface (below 40 cm depth), the travel time and amplitude variations in the reference scan are on the order of ± 0.7% and ± 35%, respectively; no trend in the variation of either attribute was apparent. Travel time changes within the glass bead layer before and after NAPL injection are nearly zero. Below the sand/bead interface, travel time changes clearly delineate the NAPL lens. Travel time changes below the NAPL lens are slightly larger than within the glass bead layer, due to NAPL residual. The magnitude of amplitude decreases due to the presence of NAPL is much greater than the variability of the water-saturated sand within the NAPL lens. Within the lens, amplitude reductions range from 60 to 95% of the amplitude through the water-saturated media; below the lens reductions range from 1 to 30%.

The measured NAPL saturation distribution from the tank excavation is shown in Figure 2(e). The distribution shown is from the vertical cross-section of the tank between the scanning boreholes. No NAPL was detected within the glass bead layer. Most of the NAPL accumulated in the top 15 cm of the coarse sand, where NAPL saturations ranged from 32% to 81% of the pore space. NAPL saturations are lower near the top of the lens (between depths 35 and 40 cm), because of the smaller pore sizes where smaller glass beads partially fill the coarse sand pores. The layers of constant saturation at the bottom of the lens were measured by freezing, consequently these values represent averages over the horizontal cross-section of the tank. Figure 2(f) shows NAPL saturation distribution below the NAPL lens at a higher resolution than in Figure 2(e). Saturations range from 0 to 16%, with maximum values corresponding to the depths of maximum amplitude change seen in Figure 2(d) at 58 and 63 cm.

The measured P-wave velocity through the middle of the NAPL layer (43 cm depth) is 1509 m/s, compared to the pre-injection value of 1760 m/s. These values were calculated from the ratio of the distance between the boreholes (50.8 cm) and the corrected travel time. Geller and Myer's (1995) model of P-wave velocity as a function of NAPL saturation, derived from Kuster and Toksöz (1974), predicts a P-wave velocity of 1759 m/s for water-saturated sand of 39.5% porosity. For the same porosity, the model predicts a dodecane saturation of 70% for a velocity of 1509 m/s. The close agreement with measured values shows that the velocities can be predicted by average NAPL saturation values, even if the saturations vary along the presumed travel path of the wave.

The decrease in amplitudes is fairly constant from the middle to the bottom of the lens (45 to 50 cm depth in Fig. 2d), while NAPL saturation decreases from 70% to 30% (Fig 2e). This suggests a non-linear relationship between saturation and attenuation. Towards the middle of the lens, the NAPL distribution is expected to be more homogeneous throughout the horizontal cross-section than near the bottom of the lens. The bottom of the lens is an irregular interface with the water-saturated media, where patches of water-saturated media occur between sections occupied by NAPL. The patchy NAPL distribution may be more attenuating compared to the same volume of NAPL that is evenly distributed throughout the cross-section. This is consistent with other observations and analyses (Geller and Myer, 1995; Seifert et al., 1998; Cadoret et al., 1998) where increased energy attenuation occurs in the presence of irregular and patchy distributions of immiscible fluids compared to lower attenuation for a more homogeneous fluid phase distributions.

Figures 3(a) and 3(b) show the zero-offset scans for Experiment B, taken in the water-saturated sand before and following the injection of the NAPL, respectively. In the post-injection scan (Fig. 3b), the presence of the NAPL causes changes in travel times, amplitudes and diffraction patterns (horizontal "v-shape" arrivals) throughout the depth of the tank.

Figures 3(c) and 3(d) plot the variation in travel times and amplitudes, respectively, with depth before and after NAPL injection. Before NAPL injection, travel times were nearly constant (±0.2%), and amplitudes (trough to peak) varied on the order of ±12% without any systematic trend. After NAPL injection, the largest travel time increase of about 1.4% occurred at around 55 cm depth. The amplitude decreased by about 40% at around 40 cm depth and nearly 70% at the same elevation where the travel time increase was observed, as measured from the first trough to peak. These amplitude changes are significantly larger than the amplitude variability in the water-saturated sand.

Figure 3(e) shows the NAPL saturation distribution in the vertical cross-section between the scanning boreholes. Saturations range from 0.01% to 8.3%, with highest values occurring at the depths of maximum amplitude decrease in Fig 3(d). The vertical discontinuity in the distribution is partially due to the three-dimensional geometry of the flow channels, which occur in and out of the plane of the cross-section. The horizontally-averaged saturations in Figure 3(f) range from 0.8 to 4.4%. The maximum saturation near 55 cm corresponds to the depth at which the maximum changes in travel time and amplitude occur (Figs. 3c and 3d).

Conclusions

The observed trends of the effect of NAPL on P-wave transmission at the tank-scale (acoustic frequencies) are consistent with behavior at the column scale (ultrasonic frequencies). P-wave velocities can be predicted by NAPL saturation using simple mixing laws. Amplitude changes are significantly greater than velocity changes, and do not appear directly predictable from NAPL saturation alone. That is, irregular and patchy NAPL distribution due to channelized flow may cause increased scattering attenuation when compared to the homogeneous distribution of immiscible phases. This form of attenuation is likely to be sensitive to the geometry of the scattering volumes. This suggests that scattering is still important at the lower frequencies of the tank-scale experiments, where the scale of liquid-phase heterogeneities is equivalent to, or greater than, the acoustic wavelength. NAPL

residual saturation changes from NAPL flow channels of 3 to 4 % were detectable, and the 40 to 80% NAPL saturation in the NAPL lens was clearly visible at acoustic frequencies. Smaller NAPL saturations had a relatively larger effect on attenuation at the tank scale compared to the column scale. This suggests that at the tank scale, propagating P-waves encounter a larger degree of heterogeneity in NAPL distribution compared to the column scale.

Acknowledgment

The authors would like to thank Larry Myer, John Peterson, Roland Gritto, and Henk Keers for their insights on wave propagation and imaging in unconsolidated media, and Larry Myer and Ernie Majer for reviewing this report. This work was sponsored by the Director, Office of Energy Research, Office of Basic Energy Sciences, Geosciences Program, through U.S. Department of Energy contracts DE-AC03-76F00098 and DEF602-93ER14391 and by the Air Force Office of Scientific Research, USAF, under grant/contract number FQ8671-96-0-1169. The views and conclusions contained herein are those of the authors and should not be interpreted as necessarily representing the official policies or endorsements, either expressed or implied, of the Air Force Office of Scientific Research or the U.S. Government.

References

Cadoret, T., G. Mavko and B. Zinszner, Fluid distribution effect on sonic attenuation in partially saturated limestones, Geophysics, 63(1), pp154-160, 1998.

Geller, J. T. and L. R. Myer, Ultrasonic imaging of organic liquid contaminants in unconsolidated porous media, Journal of Contaminant Hydrology, 19(3), pp85-104, 1995.

Keers, H., L. Johnson and D. Vasco, Crosswell imaging using asymptotic waveforms, submitted to Geophysics, 1999.

Kowalsky, M. B., J. T. Geller, P. K. Seifert, K. T. Nihei, R. Gritto, J. E. Peterson, Jr. and L. R. Myer, Acoustic visibility of immiscible liquids in poorly consolidated sand, 1998 International Exposition and 68th Annual Convention, Society of Exploration Geophysics, New Orleans, LA, pp1041-1044, 1998.

Kuster, G. T. and Toksöz, M. N., Velocity and attenuation of seismic waves in two-phase media; Part I-Theoretical formulations, Geophysics, 39(5), pp587-606, 1974.

Riddick, J. A. and Bunger, W. B., Organic Solvents – Physical Properties and Methods of Purification, Wiley-Interscience, New York, NY 3rd ed., 1970.

Seifert, P. K., J. T. Geller and L. R. Johnson, Effect of P-wave scattering on velocity and attenuation in unconsolidated sand saturated with immiscible liquids, Geophysics, 63(1), pp161-170, 1998.

Wang, Z. and Nur, A., Ultrasonic velocities in pure hydrocarbons and mixtures, J. Acoust. Soc. Am., 89(6), pp2725-2730, 1991.

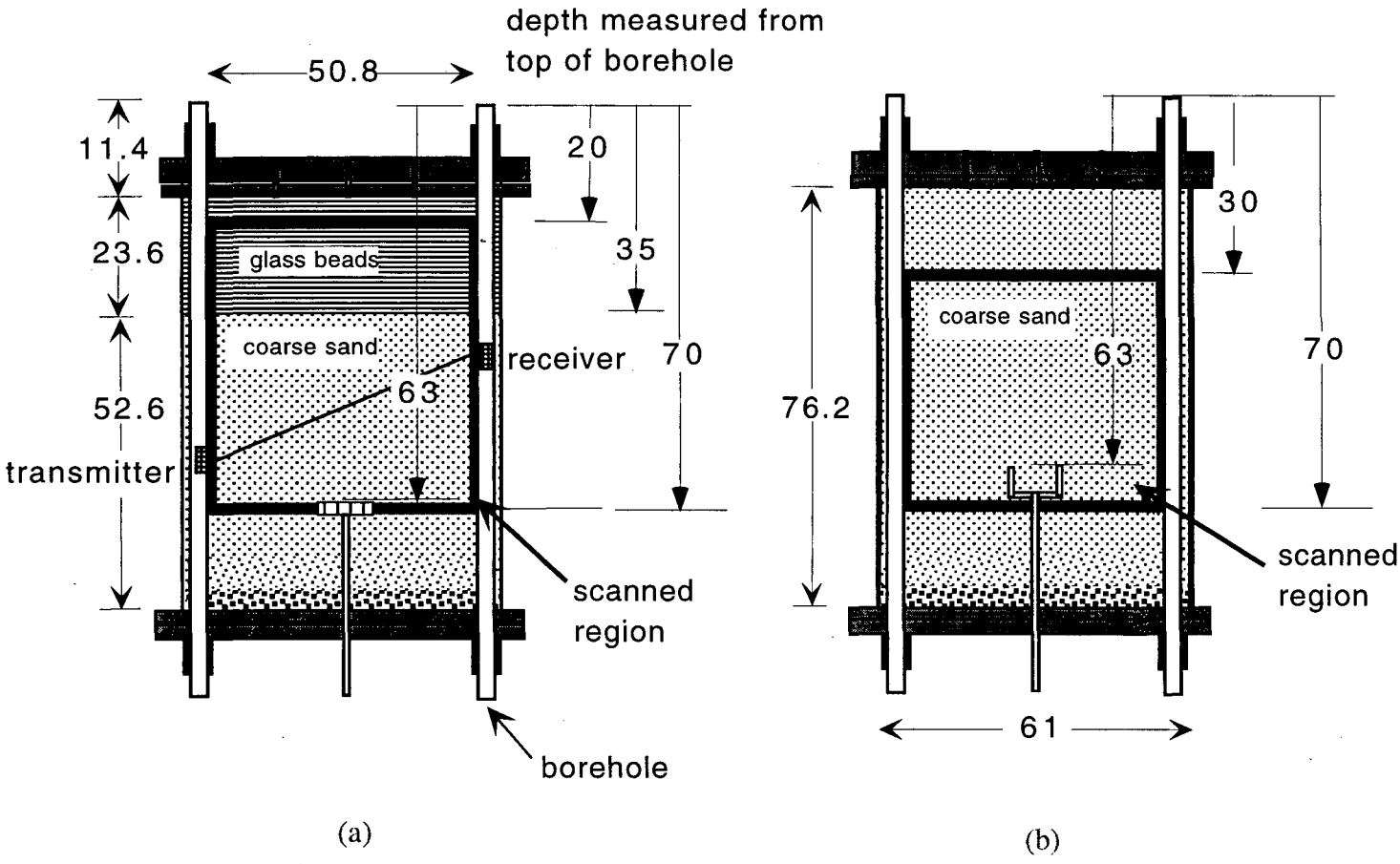

Figure 1. Vertical cross sections of experimental tank. All dimensions are in cm. (a) Experiment A for NAPL lens (b) Experiment B for NAPL residual

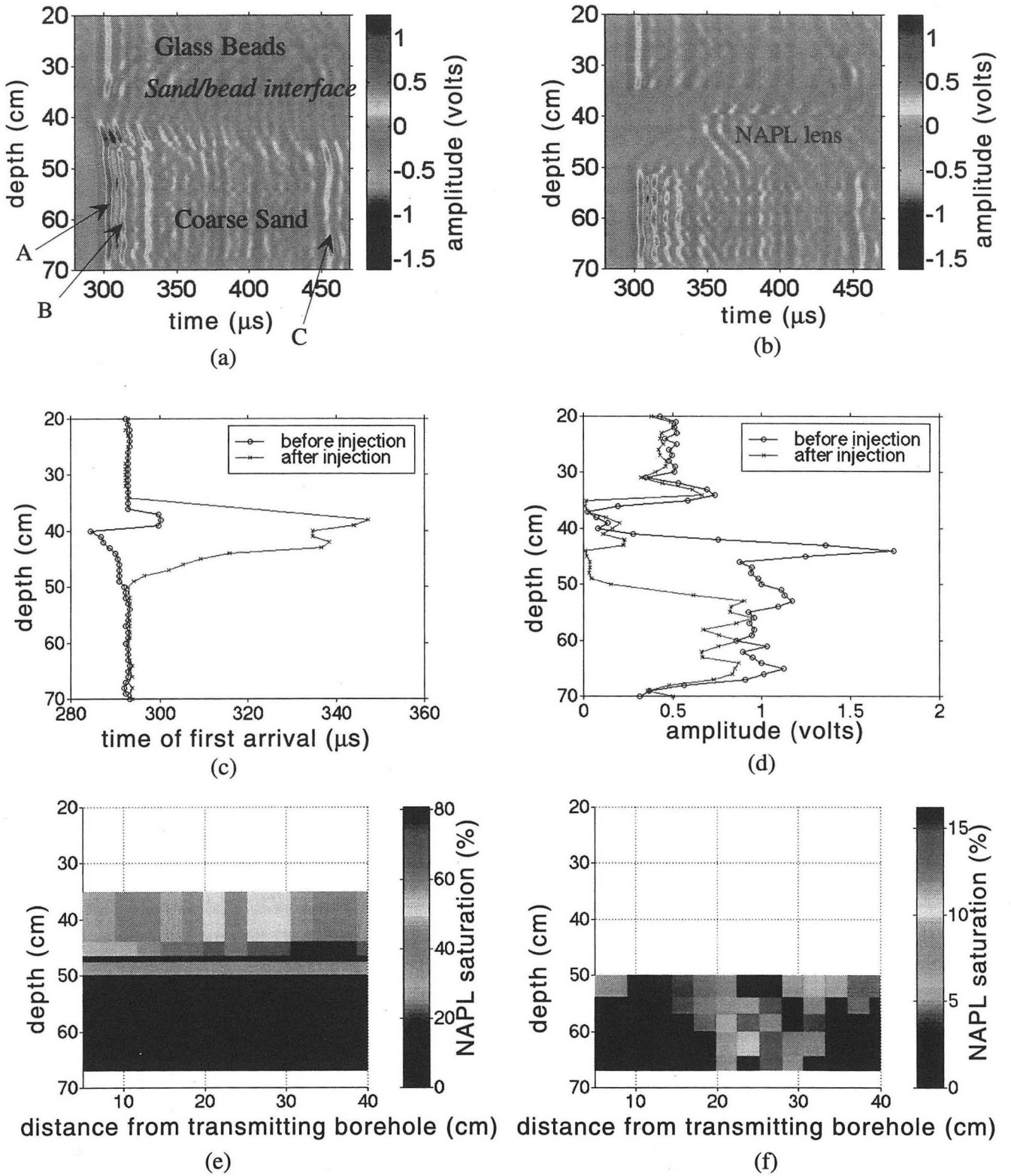

Figure 2. Results for Experiment A, detection of NAPL lens. (a) Zero offset scan of water-saturated sand, arrow A indicates time of first arrival, B indicates reflection off tank wall adjacent to borehole and C indicates reflection off tank side, (b) Zero offset scan following the injection of n-dodecane, (c) First arrival times for before and after NAPL injection, (d) Amplitudes (trough to peak) before and after NAPL injection, (e) NAPL saturation distribution in scanning plane from tank excavation, (f) Increased resolution of NAPL saturation distribution below lens.

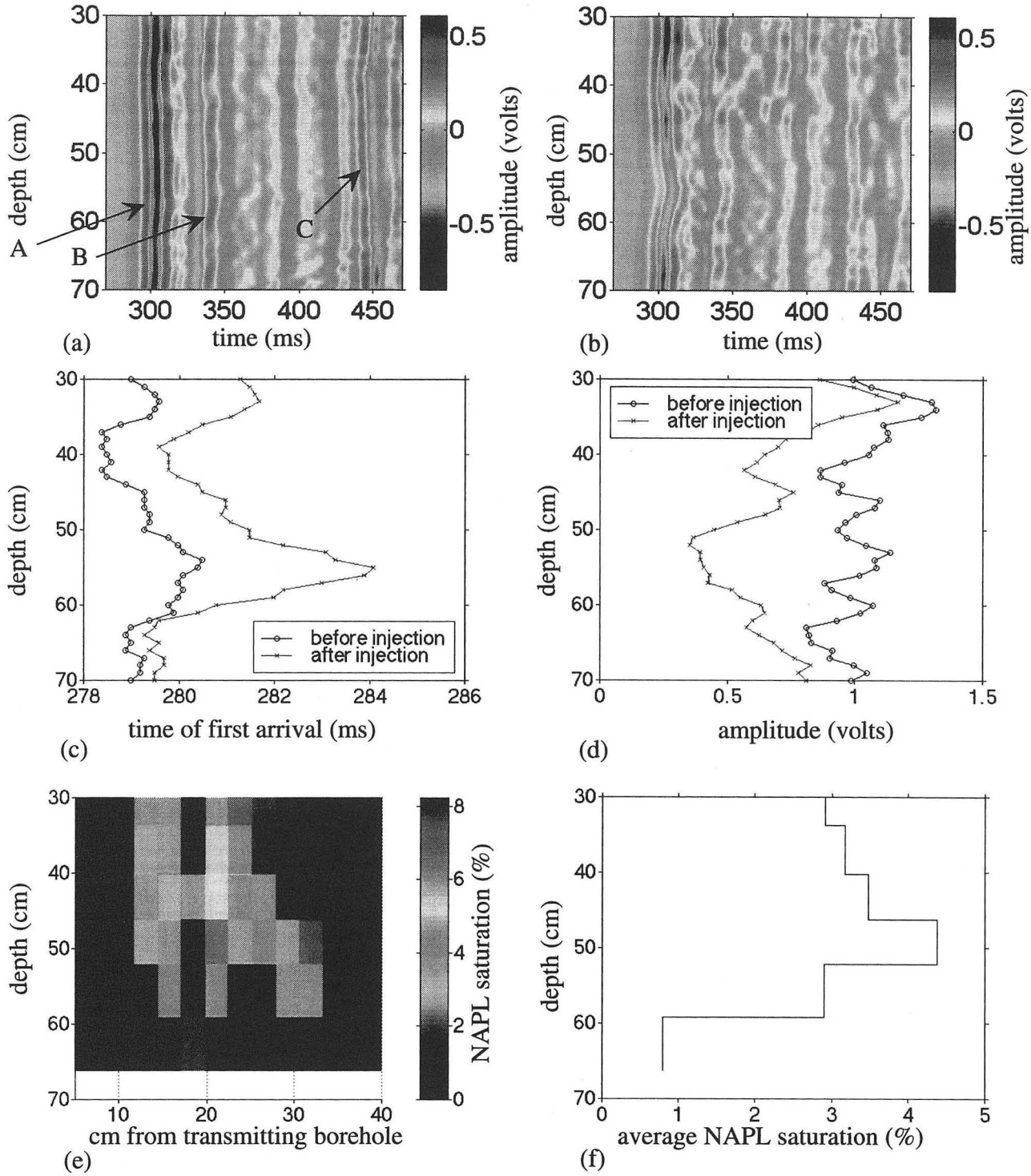

Figure 3. Results for Experiment B, detection of NAPL residual. (a) Zero offset scan of water-saturated sand, arrow A indicates time of first arrival, B indicates reflection off tank wall adjacent to borehole and C indicates reflection off tank side, (b) Zero offset scan following the injection of n-dodecane, (c) First arrival times for before and after NAPL injection, (d) Amplitudes (trough to peak) before and after NAPL injection, (e) NAPL saturation distribution in scanning plane from tank excavation, (f) Horizontally averaged NAPL saturation in scanning plane.

Ernest Orlando Lawrence Berkeley National Laboratory
One Cyclotron Road | Berkeley, California 94720

Prepared for the U.S. Department of Energy under Contract No. DE-AC03-76SF00098